

Geometric Graph Learning with Extended Atom–Types Features for Protein–Ligand Binding Affinity Prediction

Md Masud Rana¹ and Duc Duy Nguyen¹ *

¹ Department of Mathematics, University of Kentucky, KY 40506, USA

January 18, 2023

Abstract

Understanding and accurately predicting protein-ligand binding affinity are essential in the drug design and discovery process. At present, machine learning-based methodologies are gaining popularity as a means of predicting binding affinity due to their efficiency and accuracy, as well as the increasing availability of structural and binding affinity data for protein-ligand complexes. In biomolecular studies, graph theory has been widely applied since graphs can be used to model molecules or molecular complexes in a natural manner. In the present work, we upgrade the graph-based learners for the study of protein-ligand interactions by integrating extensive atom types such as SYBYL and extended connectivity interactive features (ECIF) into multiscale weighted colored graphs (MWCG). By pairing with the gradient boosting decision tree (GBDT) machine learning algorithm, our approach results in two different methods, namely ^{sybyl}GGL-Score and ^{ecif}GGL-Score. Both of our models are extensively validated in their scoring power using three commonly used benchmark datasets in the drug design area, namely CASF-2007, CASF-2013, and CASF-2016. The performance of our best model ^{sybyl}GGL-Score is compared with other state-of-the-art models in the binding affinity prediction for each benchmark. While both of our models achieve state-of-the-art results, the SYBYL atom-type model ^{sybyl}GGL-Score outperforms other methods by a wide margin in all benchmarks.

Keywords— geometric graph learning, protein-ligand binding affinity, atom-type interaction, weighted colored sub-graph, machine learning

1 Introduction

In recent years, graph theories have been widely used in chemical, biological, physical, social, and computer sciences. This is because graphs are useful for representing and analyzing a wide range of practical problems. In molecular modeling, graph representation is widely used since it is a natural way to model their structures, in which graph vertices represent atoms and graph edges represent possible interactions between them. In general, graph theories can be divided into three categories: geometric graph theory, algebraic graph theory, and topological graph theory. Geometric graph theory studies a graph’s geometric connectivity, which refers to the pairwise relations among graph nodes or vertices [1]. Algebraic graph theory concerns the algebraic connectivity via the characteristic polynomial, eigenvalues, and eigenvectors of matrices associated with the graph, such as the adjacency matrix or the Laplacian matrix [2, 3]. In topological graph theory, embedding and immersion of graphs are studied along with their association with topological spaces, such as abstract simplicial complexes [4, 5].

There are numerous applications of graphs in chemical analysis and biomolecular modeling [6, 7, 8, 9], such as normal-mode analysis (NMA) [10, 11, 12, 13] and elastic network model (ENM) [14, 15, 16, 17, 18, 19] used to study protein B–factor prediction. Algebraic graph theory has been utilized in some of the most popular elastic network models (ENMs) such as the Gaussian network model (GNM) and the anisotropic network model (ANM). However, due to the matrix-diagonalization procedure, these methods have a computational complexity of $\mathcal{O}(N^3)$, with N being the number of matrix elements. Furthermore, these methods suffer from limited accuracy in protein B–factor prediction, with average Pearson correlation coefficients less than 0.6 in all datasets. A geometric graph theory-based weighted graph approach, called flexibility-rigidity index (FRI), was introduced to bypass matrix diagonalization in GNM [20, 21, 22, 23]. FRI assumes that protein interactions, including interactions with its environment, completely determine its structure in a given environment, which in turn, fully determines protein flexibility and functions. Therefore, it is not necessary to invoke a high-dimensional protein interaction Hamiltonian as in spectral graph theory to analyze protein flexibility when the accurate structure of the protein and its environment are known. While the computational complexity of earlier FRI [20] is of $\mathcal{O}(N^2)$, the fast FRI [21] is of $\mathcal{O}(N)$. In order to capture multiscale interactions in macromolecules, multiscale FRI (mFRI) was introduced [24], resulting in a number of graphs with parallel edges, i.e. multiple graphs. Despite the fact that mFRI is about 20% more accurate than the GNM on a set of 364 proteins, the average Pearson’s correlation coefficient in B–factor prediction falls below 0.7, which is insufficient to provide a reliable assessment of protein flexibility. The limited accuracy of these graph-based models is due to the fact that they do not distinguish different chemical element types in a molecule or biomolecule, resulting in a severe loss of important chemical and biological information.

*Address correspondences to Duc Duy Nguyen. E-mail: ducnguyen@uky.edu

To address the aforementioned problem, a multiscale weighted colored graph (MWCG) model was introduced for protein flexibility analysis [25]. In MWCG, the graph of a protein structure is colored according to the type of interaction between nodes in the graph, and subgraphs are defined according to colors. This process is commonly referred to as graph coloring, which is an important technique in graph theory that allows graph vertices or edges to be treated differently. MWCG weights the importance of graph edges by scaling their Euclidean distances in radial basis functions so that the nearest neighbors have the strongest edges in the sense of the Euclidean metric. Mathematical properties of MWCGs include low dimensionality, simplicity, robustness, and invariance of rotations, translations, and reflections. Subgraphs constructed from vertex-labeled and edge-labeled graphs provide powerful representations of intermolecular and intramolecular interactions, such as hydrogen bonds, electrostatics, van der Waals interactions, hydrophilicity, hydrophobicity, etc [1, 25]. The MWCG models offer 40% more accuracy than the GNM in protein B-factor prediction [25].

Molecular interactions between proteins and substrate molecules (ligands) are the principal determinant of many vital processes, such as cellular signaling, transcription, metabolism, and immunity. Therefore, understanding protein-ligand interactions is a central issue in biochemistry, biophysics, and molecular biology. Moreover, an accurate prediction of protein-ligand binding affinity plays a critical role in computational drug design, particularly in virtual screening and lead optimization. Various scoring functions (SFs) have been developed over the past few decades to evaluate protein-ligand interactions in structure-based drug design. These SFs can be classified mainly into four categories: force-field-based or physics-based SF, empirical SF, knowledge-based SF, and machine-learning-based SF. Force-field-based SFs offer physical insight and are not dependent on existing data. Empirical SFs utilize a number of physical sub-models and use regression to fit existing data. The knowledge-based SF uses available datasets to derive binding patterns for proteins and ligands without requiring further training. Finally, machine learning-based SFs are data-driven, and are capable of capturing non-linear and complex relationships in the data. They can also easily handle large and diverse datasets. The performance of machine learning-based SFs strongly depends on the training set, in addition to their descriptors and machine learning algorithms. These scoring functions often take the top place in several standard benchmarks and community-wide competitions [26, 27, 28, 29, 30].

In recent years, due to the increasing availability of structural and binding affinity data for protein-ligand complexes, machine-learning SFs have become increasingly popular for binding affinity prediction. The RF-Score [31] is considered one of the first machine-learning-based SFs to outperform other SFs in the CASF-2007 benchmark dataset. The model uses the random forest algorithm and employs element-type pair counts as features to describe protein-ligand complexes. The model was later extended to incorporate a more precise chemical description, including SYBYL atom-type pair counts features [32]. Including SYBYL atom types into the model permits deconvoluting the element into a hybridization state and bonding environment. For example, instead of having a single Carbon (C) element atom type, the SYBYL scheme allows the following subtypes: C.1, C.2 C.3, C.ar, and C.cat. A number of SYBYL atom-type-based models have been developed in the past years [33], including SYBYL::ChemScore, SYBYL::G-Score, and SYBYL::D-Score. In a separate study, it has been shown that the connectivity of the atoms [34] can improve the performance of a machine learning model in the binding affinity prediction task [35]. In [35], the authors used a set of protein-ligand atom-type pair counts features, called the extended connectivity interactive features (ECIF), that considers each atom’s connectivity to define the atoms involved in the pairs. The atom definition in ECIF is based on the atom environment concept initially introduced in the development of Extended Connectivity Fingerprints (ECFP) [36]. Paired with a machine learning algorithm, the ECIF model significantly improves the performance of the binding affinity prediction with Pearson’s correlation of 0.866 for the CASF-2016 benchmark. A number of machine-learning-based SF with different types of descriptors including differential geometry [37, 38], persistent homology [39, 5], and graph theory [1, 2] have emerged in the past few years for protein-ligand binding affinity prediction. Among them, the element-type graph coloring-based MWCG descriptors have particularly been successful in the task [1, 2].

In the present work, we propose a geometric graph theory-based multiscale weighted colored graph (MWCG) descriptors for the protein-ligand complex where the graph coloring is based on SYBYL atom-type and ECIF atom-type connectivity. By pairing with the advanced machine learning architectures, our approach results in two different methods, namely $^{sybyl}GGL$ -Score and ^{ecif}GGL -Score. We verify the scoring power of our proposed model against three commonly used benchmarks in drug design, namely CASF-2007 [33], CASF-2013 [40], and CASF-2016 [41]. Several experiments confirm that both of our models achieve state-of-the-art results and outperform other models by a wide margin.

2 Methods and Materials

2.1 Multiscale Weighted Colored Geometric Subgraphs

A graph \mathcal{G} of a biomolecule consists of a set of vertices \mathcal{V} and edges \mathcal{E} and can be used to describe the noncovalent interaction of atoms in the molecule. In recent years, graph theory descriptors of protein-ligand binding interactions have been developed for massive and diverse datasets [2, 42]. To improve the graph theory representation, different types of elements are labeled, which is known as graph coloring. A colored graph is used to encode different types of interactions between atoms and gives rise to a basis for the collective coarse-grained description of the dataset. Labeled atoms of a molecule are classified into subgraphs where colored edges correspond to element-specific interactions.

To account for details of physical interactions in protein-ligand complexes such as hydrophobic, hydrophilic, etc., we are interested in constructing the subgraphs in an atomic interactive manner. In our previous work [1, 2], we used the combination of the element symbols of the interacting protein-ligand atoms to classify the interaction, e.g., C-C or N-O. In the present work, instead of the element symbol, we consider the following two schemes to classify the atomic interaction. In the first approach, we consider atom name (excluding hydrogen) for protein and SYBYL atom type

for the ligand to define a range of protein-ligand atom pairs, e.g CD1–C.2, CG–C.ar, OE1–N.am, etc. In the second scheme, we consider the extended connectivity interaction features (ECIF) described in [35] to extract the protein-ligand atom-type pair that takes each atom’s connectivity into account. The ECIF atom type in a molecule is defined by considering six atomic features: atom symbol, explicit valence, number of attached heavy atoms, number of attached hydrogens, aromaticity, and ring membership. Each of these properties can be represented textually where each property is separated by a semicolon. For example, the ECIF atom type for the α carbon CA is C;4;3;1;0;0.

For convenience, let \mathcal{T} be the set of all interested atom types in a given biomolecular dataset for either of the two schemes described above. To reduce the notation complexity, we denote the atom type at the i th position in the set \mathcal{T} as \mathcal{T}_i . Assuming that a biomolecule has N atoms of interest, we denote

$$\mathcal{V} = \{(\mathbf{r}_i, \alpha_i) | \mathbf{r}_i \in \mathbb{R}^3; \alpha_i \in \mathcal{T}; i = 1, 2, \dots, N\} \quad (1)$$

a subset of N atoms (i.e. subgraph vertices) that are members of \mathcal{T} . Note that the i th atom is labeled by both its coordinate \mathbf{r}_i and atom type α_i . We assume that all the pairwise non-covalent interactions between atom types \mathcal{T}_k and $\mathcal{T}_{k'}$ in a molecule or molecular complex can be represented by fast-decay weight functions

$$\mathcal{E} = \{\Phi(\|\mathbf{r}_i - \mathbf{r}_j\|; \eta_{kk'}) | \alpha_i = \mathcal{T}_k, \alpha_j = \mathcal{T}_{k'}; i, j = 1, 2, \dots, N; \|\mathbf{r}_i - \mathbf{r}_j\| \leq c\}, \quad (2)$$

where $\|\mathbf{r}_i - \mathbf{r}_j\|$ is the Euclidean distance between the i th and j th atom and c is a predefined cutoff distance that defines the binding site of the atom type \mathcal{T}_k and $\mathcal{T}_{k'}$. Here $\eta_{kk'}$ is a characteristic distance between the atoms, and Φ is a subgraph weight that satisfies the following admissibility conditions

$$\Phi(\|\mathbf{r}_i - \mathbf{r}_j\|; \eta_{kk'}) = 1, \quad \text{as } \|\mathbf{r}_i - \mathbf{r}_j\| \rightarrow 0, \quad (3)$$

$$\Phi(\|\mathbf{r}_i - \mathbf{r}_j\|; \eta_{kk'}) = 0, \quad \text{as } \|\mathbf{r}_i - \mathbf{r}_j\| \rightarrow \infty, \quad (4)$$

$$\alpha_i = \mathcal{T}_k, \alpha_j = \mathcal{T}_{k'}.$$

Although most radial basis functions can be used as the subgraph weight, the generalized exponential function

$$\Phi_E(\|\mathbf{r}_i - \mathbf{r}_j\|; \eta_{kk'}) = e^{-(\|\mathbf{r}_i - \mathbf{r}_j\|/\eta_{kk'})^\kappa}, \quad \kappa > 0,$$

and the generalized Lorentz function

$$\Phi_L(\|\mathbf{r}_i - \mathbf{r}_j\|; \eta_{kk'}) = \frac{1}{1 + (\|\mathbf{r}_i - \mathbf{r}_j\|/\eta_{kk'})^\kappa}, \quad \kappa > 0,$$

were shown to work very well for biomolecules [21]. Now, we have a weighted colored subgraph $G(\mathcal{V}, \mathcal{E})$ for a molecule or a molecular complex and we can use it to construct atomic-level collective molecular descriptors. We define the multiscale weighted colored geometric subgraph (MWCGS) interaction between k th atom type \mathcal{T}_k and k' th atom type $\mathcal{T}_{k'}$ by

$$\mu^G(\eta_{kk'}) = \sum_i \mu_i^G(\eta_{kk'}) = \sum_i \sum_j \Phi(\|\mathbf{r}_i - \mathbf{r}_j\|; \eta_{kk'}), \quad (5)$$

$$\alpha_i = \mathcal{T}_k, \alpha_j = \mathcal{T}_{k'},$$

where $\mu_i^G(\eta_{kk'})$ is the geometric subgraph centrality for the i th atom of type \mathcal{T}_k and all atoms of type $\mathcal{T}_{k'}$. The summation over the geometric centrality $\mu_i^G(\eta_{kk'})$ in equation (5) can be interpreted as the total interaction strength for the selected atom type pair \mathcal{T}_k and $\mathcal{T}_{k'}$, which provides the atomic-level coarse-grained description of the molecular properties. The equation (5) is a generalization of a bipartite subgraph discussed in [1] for the predictions of protein-ligand binding affinities and free energy ranking. A bipartite subgraph of a protein-ligand complex is a graph in which each of its edges connects one atom in the protein and another in the ligand. We intend to capture the hydrogen bonds, polarization, electrostatics, van der Waals interactions, hydrophilicity, hydrophobicity, etc. of a protein-ligand complex through the bipartite graph coloring, i.e., atom-specific descriptions and subgraph weight.

The multiscale behavior of the MWCGS arises when a different selection of the characteristic distance $\eta_{kk'}$ for a pair of atom types k and k' are considered. Therefore, for a molecule or a biomolecule, the MWCGS allows us to systematically construct a family of collective, scalable, multiscale graph-based descriptors by an appropriate selection of atom types pair k and k' , characteristic distance $\eta_{kk'}$, and subgraph weight Φ . An illustration of the weighted colored subgraph under the SYBYL atom-type system for the molecule xanthine ($C_5H_4N_4O_2$) is presented in Figure 1.

2.2 Geometric Graph Learning

The multiscale weighted colored geometric subgraph (MWCGS) descriptors for a molecule or molecular complex can be paired with any machine learning or deep learning algorithm to predict molecular properties. In a supervised machine learning algorithm (either classification or regression), the labeled dataset is divided into two parts: a training set and a test set. Let \mathcal{X}_i be a labeled dataset for the i th molecule or molecular complex in the training set. Furthermore, suppose $\mathcal{G}(\mathcal{X}_i, \lambda)$ be a function that encodes the geometric information of the molecule or molecular complex into suitable graph representations with a set of parameters λ . The training of a machine learning model can be translated into a minimization problem,

$$\min_{\lambda, \theta} \sum_{i \in I} \mathcal{L}(\mathbf{y}_i, \mathcal{G}(\mathcal{X}_i, \lambda); \theta) \quad (6)$$

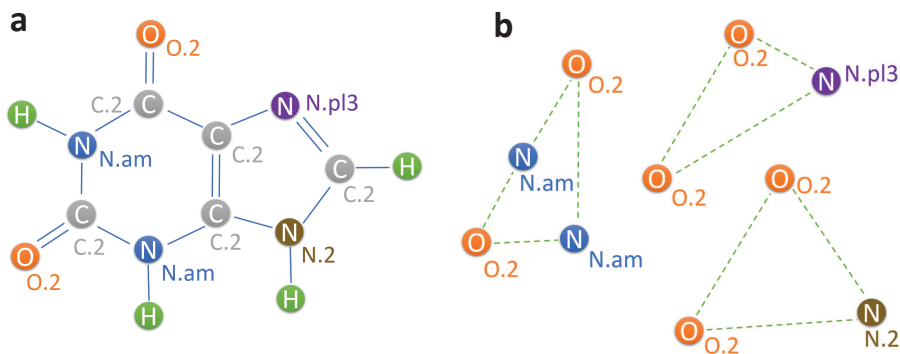


Figure 1: Illustration of the weighted colored subgraph. Part (a) is a diagram of the structure of the xanthine molecule ($C_5H_4N_4O_2$; ligand name: XAN; PDB ID: 2uz9), and (b) the weighted colored subgraphs, from left to right, $G_{N.am-O.2}$, $G_{N.pl3-O.2}$, and $G_{N.2-O.2}$ consisting of SYBYL atom-type pair N.am-O.2, N.pl3-O.2, and N.2-O.2, respectively. The dashed line in (b) represents the edges of the graph.

where \mathcal{L} is a scalar loss function to be minimized and \mathbf{y}_i is the labels of the i th sample in the training set I . Here, θ is the set of hyperparameters that depends on the chosen machine learning algorithm and typically be optimized for optimal performance. A wide range of machine learning algorithms, such as support vector machines, random forests, gradient boosting trees, artificial neural networks, and convolution neural networks, can be implemented in conjugation with the present geometric subgraph descriptors. However, to focus on the descriptive power of the proposed geometric subgraph features, we only employ gradient boosting decision trees (GBDT) in the present work and avoid optimizing machine learning algorithm selections. Although relatively simple, GBDT is still powerful, robust against overfitting, and a widely used ensemble algorithm. An illustration of the proposed geometric graph learning strategy is presented in Figure 2.

We use GBDT module in scikit-learn v0.24.1 package with the following parameters: `n_estimators` = 20000, `max_depth` = 8, `min_samples_split` = 2, `learning_rate` = 0.005, `loss` = ls, `subsample` = 0.7, and `max_features` = sqrt. These parameter values are selected from the extensive tests on PDBbind datasets and are uniformly used in all our validation tasks in this work.

2.3 Dataset

For protein-ligand binding affinity prediction, the most commonly used benchmarks are the PDBbind datasets. In this work, we use the three most popular PDBbind benchmark datasets, CASF-2007, CASF-2013, and CASF-2016, to test the performance of our model. The PDBbind datasets consist of a general set, a refined set, and a core set, where the latter set is a subset of the previous one. In the present work, we explore two different training sets to build predictive models for the binding affinity of the complexes in the test set, which is the core set of the corresponding benchmark. The first training set, denoted by S_R , is the refined set excluding the core set of the corresponding benchmark. As a second training set, denoted by S_G , we use the general set excluding the core set of the corresponding benchmark. More information about these datasets is offered on the PDBbind website <http://pdbbind.org.cn/>. A summary of the dataset is provided in Table 1.

Table 1: Summary of PDBbind datasets used in the present work.

Dataset	$ S_G $	$ S_R $	$ S_C $
CASF-2007 benchmark	2852	1105	195
CASF-2013 benchmark	11713	3516	195
CASF-2016 benchmark	12998	3772	285

$|S_G|$: Number of complexes in the general set excluding the core set of the corresponding benchmark.

$|S_R|$: Number of complexes in the refined set excluding the core set of the corresponding benchmark.

$|S_C|$: Number of complexes in the core set of the corresponding benchmark.

2.4 Model Parametrization

For the sake of convenience, we use the notation $GGL_{\kappa,\tau}^\alpha$ to indicate the geometric graph learning features generated by using kernel type α and corresponding kernel parameters κ and τ . Here, $\alpha = E$ and $\alpha = L$ refer to the generalized exponential and generalized Lorentz kernels, respectively. And τ is used such that $\eta_{kk'} = \tau(\bar{r}_k + \bar{r}_{k'})$, where \bar{r}_k and $\bar{r}_{k'}$

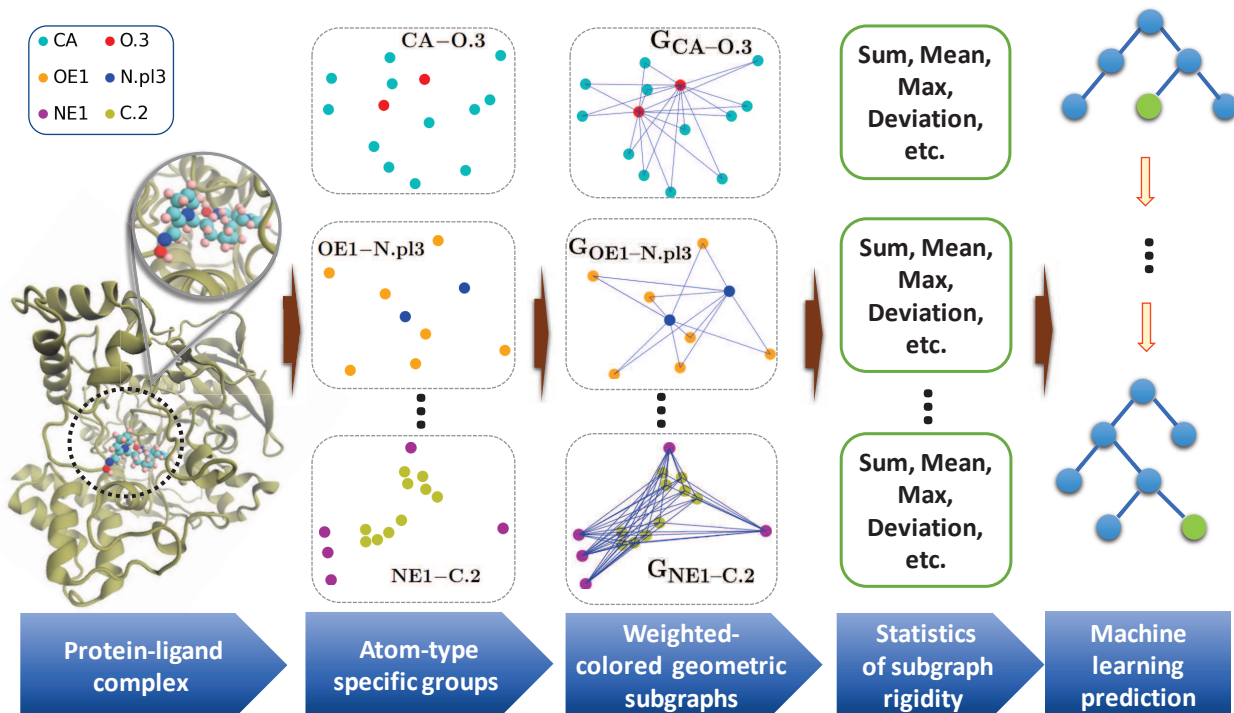


Figure 2: Illustration of the geometric graph learning strategy using the molecular complex with PDBID: 5bwc (first column). The second column represents the protein-ligand atom-type pair CA-O.3, OE1-N.pl3, and NE1-C.2, respectively from top to bottom. The corresponding weighted colored geometric subgraphs are shown in the third column. The fourth column presents the statistics of the subgraph rigidity. In the final column, the advanced machine learning models such as the gradient boosting trees integrate these statistical features for training and prediction.

are the van der Waals radii of atom type k and atom type k' , respectively. Kernel parameters κ and τ are selected based on the cross-validation with a random split of the training data. We propose a GGL representation in which multiple kernels are parametrized at different scale (η) values. In this work, we consider at most two kernels. As a straightforward notation extension, two kernels can be parametrized by $\text{GGL}_{\kappa_1, \tau_1; \kappa_2, \tau_2}^{\alpha_1, \alpha_2}$. Each of these kernels gives rise to one set of features. Finally, as we consider two different schemes to extract the protein-ligand atom-type pair, we introduce the following two notations $^{\text{sybyl}}\text{GGL}_{\kappa_1, \tau_1; \kappa_2, \tau_2}^{\alpha_1, \alpha_2}$ and $^{\text{ecif}}\text{GGL}_{\kappa_1, \tau_1; \kappa_2, \tau_2}^{\alpha_1, \alpha_2}$.

3 Results and Discussion

In this section, we present the scoring power of our proposed geometric graph learning (GGL) model for the benchmark datasets discussed above.

3.1 Hyperparameter Optimization and Model Performance

It is a well-known fact that the performance of a machine-learning model depends on the optimization of its essential parameters. To achieve the best performance of our GGL model on each benchmark, we optimize the kernel parameters κ and τ . We use five-fold cross-validation (CV) and a grid search method to find the optimal parameters τ in the range $[0.5, 10]$ and κ in the range $[0.5, 20]$ with an increment of 0.5 for both parameter ranges. The high values of the power parameter κ are considered to approximate the ideal low-pass filter (ILF) [43].

As a general strategy to optimize the model hyperparameters on each benchmark, we carry out a five-fold CV on the training set S_R which is the refined set excluding the core set of the corresponding benchmark. Once we find the best model for each benchmark dataset, we test the performance of the model on the test set S_C (i.e., the core set of the corresponding benchmark). For the prediction task, our first strategy is to train the model using the training set S_R (i.e., the refined set excluding the core set) and observe the performance on the test set. And secondly, we train the best model using the training set S_G (i.e., the general set excluding the core set) and test the performance on the test set. As the general set of each benchmark contains more diverse complexes than the refined set, we expect our model performs better when trained with the training set S_G . Below we discuss the optimization of our model hyperparameters τ and κ and the model’s performance on each benchmark.

3.1.1 CASF-2016

The first benchmark we consider is the CASF-2016, the latest of the three benchmark datasets in the PDBbind database. We carry out five-fold cross-validation (CV) on the first training set which is the refined set excluding the core set of this benchmark. The CV results for both the single-scale and two-scale SYBYL atom-type GGL models are presented in Figure 3. The parameter set $(\kappa, \tau) = (2.5, 1.5)$ gives the best median Pearson’s correlation coefficient $R_p=0.795$ for the single-scale exponential kernel (Figure 3a). For the single-scale Lorentz kernel model the parameters are $(\kappa, \tau) = (14.0, 1.5)$ with median $R_p=0.795$ (Figure 3b). The two-scale kernel model is built on top of the previously optimized single-scale kernel parameters, so we only optimize the parameters for the second kernel. Figure 3c and Figure 3d plots the CV results for the second kernel parameters κ_2 and τ_2 of the two-scale kernel SYBYL atom-type model ${}^{\text{sybyl}}\text{GGL}_{\kappa_1, \tau_1; \kappa_2, \tau_2}^{\alpha_1, \alpha_2}$ with κ_1 and τ_1 fixed at the optimal value from single-scale model. We observe that the best two-scale exponential kernel model is ${}^{\text{sybyl}}\text{GGL}_{2.5, 1.5; 15.0, 8.5}^{\text{E}, \text{E}}$ with median $R_p=0.796$ (Figure 3c) and the best two-scale Lorentz kernel model is ${}^{\text{sybyl}}\text{GGL}_{14.0, 1.5; 16.0, 0.5}^{\text{L}, \text{L}}$ with median $R_p=0.797$ (Figure 3d).

To find the optimal parameters for the ECIF atom-type models, we carry out a similar process discussed above. Figure 4 plots the CV performance of the single-scale kernel ECIF atom-type model ${}^{\text{ecif}}\text{GGL}_{\kappa, \tau}^{\alpha}$. We find that the best parameters for the single-scale exponential kernel model are $\kappa=13.0$ and $\tau=2.5$ with median $R_p=0.790$ (Figure 4a) and the best parameters for the single-scale Lorentz kernel model are $\kappa=14.0$ and $\tau=1.5$ with median $R_p=0.789$ (Figure 4b). The optimal parameters for the two-scale kernel model are also explored in a similar fashion as above. The CV results of each combination of the second kernel parameters are presented in Figure 4. The figure confirms that the best two-scale exponential kernel model is ${}^{\text{ecif}}\text{GGL}_{13.0, 2.5; 15.0, 9.0}^{\text{E}, \text{E}}$ with median $R_p=0.792$ (Figure 4c) and the best two-scale Lorentz kernel model is ${}^{\text{ecif}}\text{GGL}_{14.0, 1.5; 13.5, 9.0}^{\text{L}, \text{L}}$ with median $R_p=0.791$ (Figure 4d).

After finding the best models for this benchmark, we are interested in validating their performance on the test set, i.e., the CASF-2016 core set. The performance is measured using the Pearson’s correlation coefficient between the predicted and the experimental binding affinities of the test set complexes. First, we train each model with the smaller training set S_R , i.e., the PDBbind v2016 refined set excluding the CASF-2016 core set. Then we use the trained model to predict the test set. To this end, we repeat the model up to 50 times and use the average of all predicted values as the final predicted set. As a second approach, we train the model with the bigger training set S_G , i.e., the PDBbind v2016 general set excluding the CASF-2016 core set. For the prediction task, we again repeat the trained model 50 times and use the average of all predictions.

The performance of the best models (both SYBYL atom-type and ECIF atom-type) on the test set are listed in Table 2. We find that the performance of all models significantly improved when the model is trained with the bigger training data S_G . The results in Table 2 indicate that the two-scale models perform slightly better than their single-scale counterparts as expected. We also observe that the SYBYL atom-type models, both single-scale and two-scale, outperform their ECIF atom-type counterparts. The best model for this benchmark is the two-scale Lorentz kernel SYBYL atom-type model ${}^{\text{sybyl}}\text{GGL}_{14.0, 1.5; 16.0, 0.5}^{\text{L}, \text{L}}$ with reported Pearson’s correlation $R_p=0.873$. In addition, we compare the scoring power of our proposed GGL-Score against various state-of-the-art scoring functions in the literature [33, 31, 44, 45, 46, 47]. Figure 9c illustrates such a comparison for CASF-2016 benchmark and clearly our model stands in the top. The second best is the TopBP-DL with reported $R_p=0.848$. It must be stressed that the base geometric and algebraic graph learning models that consider the element-specific interactions instead of the atom-type interactions have a comparatively lower performance with $R_p=0.815$ [1] and $R_p=0.835$ [2] respectively. The above comparison and Figure 9c confirm the scoring power and the effectiveness of considering atom-type pair interactions in the present model. Moreover, to highlight that the current model’s impressive performance is due to the incorporation of the atom-type pair interactions and not because of the use of larger training data S_G , we explore the performance of the base GGL models with element-specific interactions that are trained on the set S_G . The details of this experiment and results are presented in Appendix 5. While the use of the bigger training data improves the performance of the base GGL model, our extended atom-type models still outperform them by a big margin (see Table A1).

Table 2: Performance of various GGL models on CASF-2016 test set.

Pearson’s R_p of single-scale Model			Pearson’s R_p of two-scale Model	
Model	Trained with S_R	Trained with S_G	Model	Trained with S_G
${}^{\text{sybyl}}\text{GGL}_{2.5, 1.5}^{\text{E}}$	0.838	0.872	${}^{\text{sybyl}}\text{GGL}_{2.5, 1.5; 15.0, 8.5}^{\text{E}, \text{E}}$	0.872
${}^{\text{sybyl}}\text{GGL}_{14.0, 1.5}^{\text{L}}$	0.832	0.872	${}^{\text{sybyl}}\text{GGL}_{14.0, 1.5; 16.0, 0.5}^{\text{L}, \text{L}}$	0.873
${}^{\text{ecif}}\text{GGL}_{13.0, 2.5}^{\text{E}}$	0.824	0.867	${}^{\text{ecif}}\text{GGL}_{13.0, 2.5; 15.0, 9.0}^{\text{E}, \text{E}}$	0.868
${}^{\text{ecif}}\text{GGL}_{14.0, 1.5}^{\text{L}}$	0.822	0.865	${}^{\text{ecif}}\text{GGL}_{14.0, 1.5; 13.5, 9.0}^{\text{L}, \text{L}}$	0.868

3.1.2 CASF-2013

As a second benchmark dataset among the CASF family, we consider the CASF-2013 benchmark. For both SYBYL atom-type and ECIF atom-type models, we carry out a similar hyperparameter optimization to that of the CASF-2016 benchmark. We use the smaller training set S_R of this benchmark which is the PDBbind v2015 refined set excluding

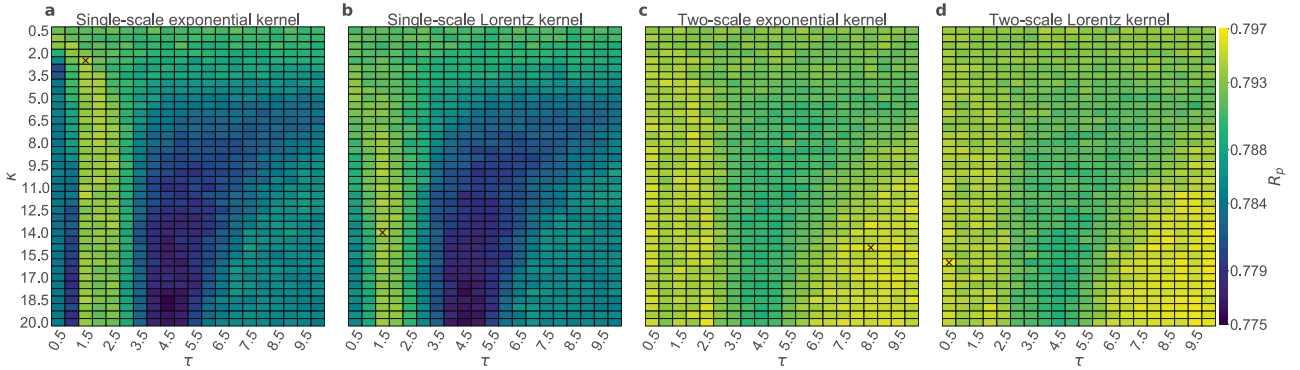


Figure 3: Optimized parameters for sybylGGL model for CASF-2016 benchmark. The best parameters locations are marked by “x”. The optimal parameters for, (a) single-scale exponential kernel model are $(\kappa, \tau) = (2.5, 1.5)$ with the corresponding median $R_p = 0.795$ and (b) single-scale Lorentz kernel model are $(\kappa, \tau) = (14.0, 1.5)$ with corresponding median $R_p = 0.795$. The optimal second kernel parameters for (c) two-scale exponential kernel model are $(\kappa, \tau) = (15.0, 8.5)$ with the corresponding median $R_p = 0.796$ and (d) two-scale Lorentz kernel model are $(\kappa, \tau) = (16.0, 0.5)$ with the corresponding median $R_p = 0.797$.

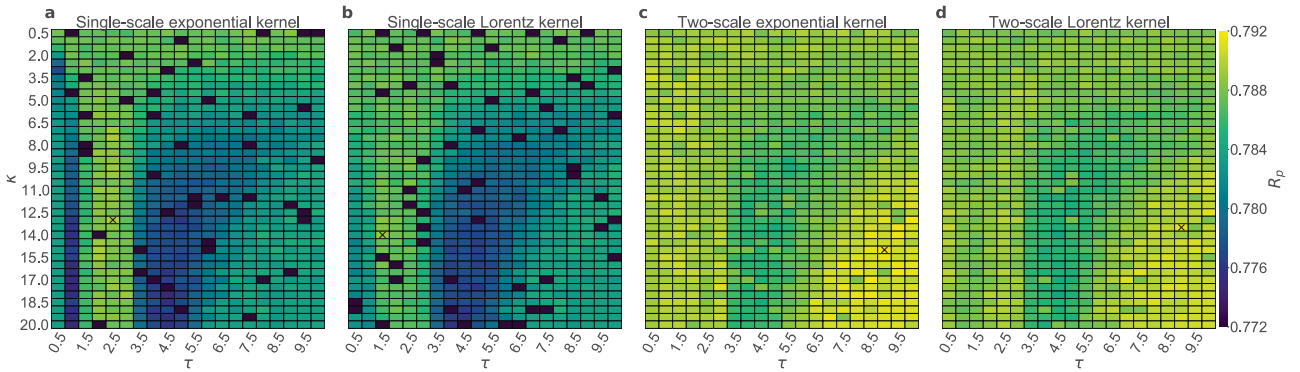


Figure 4: Optimized parameters for ecifGGL model for CASF-2016 benchmark. The best parameters locations are marked by “x”. The optimal parameters for (a) single-scale exponential kernel model are $(\kappa, \tau) = (13.0, 2.5)$ with the corresponding median $R_p = 0.790$ and (b) single-scale Lorentz kernel model are $(\kappa, \tau) = (14.0, 1.5)$ with corresponding median $R_p = 0.789$. The optimal second kernel parameters for (c) two-scale exponential kernel model are $(\kappa, \tau) = (15.0, 9.0)$ with the corresponding median $R_p = 0.792$ and (d) two-scale Lorentz kernel model are $(\kappa, \tau) = (13.5, 9.0)$ with the corresponding median $R_p = 0.791$.

the CASF-2013 core set for the cross-validation process. Figure 5 reveals the optimal parameters for the SYBYL atom-type model. The best parameters for the single-scale exponential kernel are found to be $\kappa=5.5$ and $\tau=2.0$ with median $R_p=0.796$ (Figure 5a) and the best parameters for the single-scale Lorentz kernel are $\kappa=5.5$ and $\tau=0.5$ with median $R_p=0.795$ (Figure 5b). For the two-scale kernel models, we fix the first kernel parameters at their optimal value and optimize the second kernel parameter. Figure 5c shows that the best two-scale exponential kernel model is $\text{sybylGGL}_{5.5,0.5;12.0,9.5}^{\text{E,E}}$ with median $R_p=0.798$ and Figure 5d shows that the best two-scale Lorentz kernel model is $\text{sybylGGL}_{5.5,0.5;12.0,9.5}^{\text{L,L}}$ with median $R_p=0.798$.

For the ECIF atom-type model hyperparameter optimization, we follow the same procedure as above. We found that the best single-scale exponential kernel model is $\text{ecifGGL}_{12.0,2.5}^{\text{E}}$ with median $R_p=0.792$ (Figure 6a) and the best single-scale Lorentz kernel model is found to be $\text{ecifGGL}_{18.0,2.0}^{\text{L}}$ with median $R_p=0.791$ (Figure 6b). For the two-scale kernel model, the best two-scale exponential kernel model is found to be $\text{ecifGGL}_{12.0,2.5;15.0,8.5}^{\text{E,E}}$ with median $R_p=0.795$ (Figure 6c). Finally, from Figure 6d, we found that the best two-scale Lorentz kernel model is $\text{ecifGGL}_{18.0,2.0;15.0,8.5}^{\text{L,L}}$ with median $R_p=0.795$.

Furthermore, we utilize the best models of this benchmark to predict the binding affinity of the 195 complexes in the CASF-2013 test set. Like the CASF-2016 benchmark, we first train each model using the smaller training set of this benchmark, i.e., the PDBbind v2015 refined set excluding the CASF-2013 core set, and then we generate a prediction for the test set from the average of 50 runs. Secondly, we use the more extensive training set, PDBbind v2015 general set, excluding the CASF-2013 core set to train the model and use it to get the prediction for the test set.

The performance of all models on the CASF-2013 test set is reported in Table 3. It is interesting to see a similar trend that the performance of all models improved significantly when the model is trained on the bigger training data S_G . We also observe that the SYBYL atom-type models consistently outperform their ECIF atom-type counterparts. With the two-scale kernel model performing slightly better than the single-scale kernel model, the best-performing model for this benchmark is the two-scale exponential kernel SYBYL atom-type model $\text{ecifGGL}_{12.0,2.5;15.0,8.5}^{\text{E,E}}$ with reported Pearson's correlation coefficient $R_p=0.848$. Additionally, Figure 9b proves the dominance of our model in the scoring power over other published models for this benchmark. The reported $R_p=0.848$ of our best model is significantly higher than the $R_p=0.808$ of the runner-up model TopBP. Furthermore, Table A1 in Appendix 5 confirms that the outstanding performance of our model is due to the incorporation of the atom-type interactions in the model.

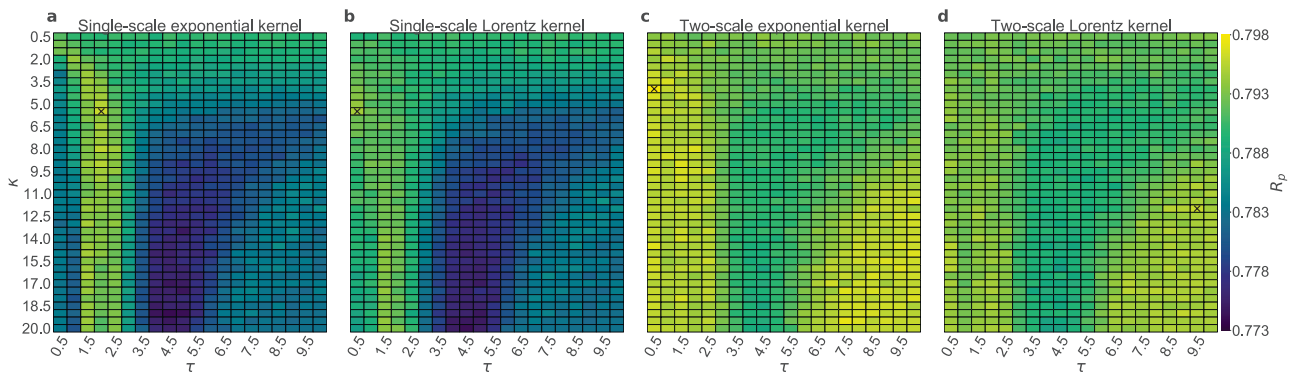


Figure 5: Optimized parameters for sybylGGL model for CASF-2013 benchmark. The best parameters locations are marked by “x”. The optimal parameters for (a) single-scale exponential kernel model are $(\kappa, \tau) = (5.5, 2.0)$ with the corresponding median $R_p = 0.796$ and (b) single-scale Lorentz kernel model are $(\kappa, \tau) = (5.5, 0.5)$ with corresponding median $R_p = 0.795$. The optimal second kernel parameters for (c) two-scale exponential kernel model are $(\kappa, \tau) = (4.0, 0.5)$ with the corresponding median $R_p = 0.798$ and (d) two-scale Lorentz kernel model are $(\kappa, \tau) = (12.0, 9.5)$ with the corresponding median $R_p = 0.798$.

Table 3: Performance of various GGL models on CASF-2013 test set.

Model	Pearson's R_p of single-scale Model		Pearson's R_p of two-scale Model	
	Trained with S_R	Trained with S_G	Model	Trained with S_G
$\text{sybylGGL}_{5.5,2.0}^{\text{E}}$	0.797	0.846	$\text{sybylGGL}_{5.5,2.0;4.0,0.5}^{\text{E,E}}$	0.848
$\text{sybylGGL}_{5.5,0.5}^{\text{L}}$	0.812	0.841	$\text{sybylGGL}_{5.5,0.5;12.0,9.5}^{\text{L,L}}$	0.844
$\text{ecifGGL}_{12.0,2.5}^{\text{E}}$	0.797	0.826	$\text{ecifGGL}_{12.0,2.5;15.0,8.5}^{\text{E,E}}$	0.829
$\text{ecifGGL}_{18.0,2.0}^{\text{L}}$	0.801	0.829	$\text{ecifGGL}_{18.0,2.0;15.0,8.5}^{\text{L,L}}$	0.833

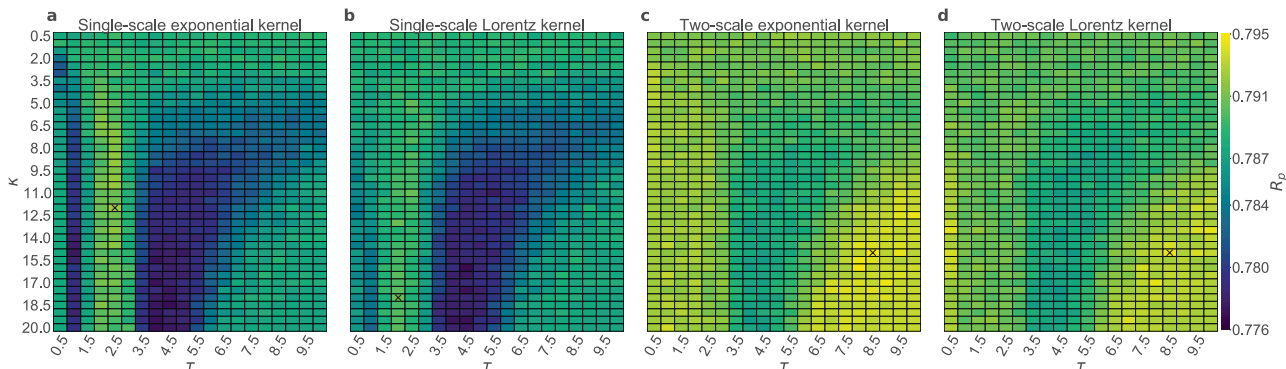


Figure 6: Optimized parameters for ecifGGL model for CASF-2013 benchmark. The best parameters locations are marked by “x”. The optimal parameters for (a) single-scale exponential kernel model are $(\kappa, \tau) = (12.0, 2.5)$ with the corresponding median $R_p = 0.792$ and (b) single-scale Lorentz kernel model are $(\kappa, \tau) = (18.0, 2.0)$ with corresponding median $R_p = 0.791$. The optimal second kernel parameters for (c) two-scale exponential kernel model are $(\kappa, \tau) = (15.0, 8.5)$ with the corresponding median $R_p = 0.795$ and (d) two-scale Lorentz kernel model are $(\kappa, \tau) = (15.0, 8.5)$ with the corresponding median $R_p = 0.795$.

3.1.3 CASF-2007

Our last benchmark is the CASF-2007. The hyperparameter optimization for this benchmark is similar to the previous two benchmarks. The smaller training set S_R , which is the PDBbind v2007 refined set excluding the CASF-2007 core set, is used for the five-fold CV. The CV performances of the SYBYL atom-type models are plotted in Figure 7. The optimal kernel parameters for the single-scale exponential model are $\kappa=2.5$ and $\tau=0.5$ (Figure 7a) with median $R_p=0.745$. For the single-scale Lorentz kernel, Figure 7b, the best parameters are $\kappa=13.5$ and $\tau=0.5$ with median $R_p=0.746$. The two-scale models are built on top of the optimized single-scale model, we only search for the optimal second kernel parameters. Figure 7c shows that the two-scale exponential model $\text{sybylGGL}_{2.5,0.5;19.0,9.0}^{\text{E,E}}$ gives the best median $R_p=0.747$ while Figure 7d reveals that the best two-scale Lorentz kernel model is $\text{sybylGGL}_{13.5,0.5;13.0,9.5}^{\text{L,L}}$ with median R_p being 0.747.

The hyperparameter optimization for the ECIF atom-type models is carried out in a similar fashion. Figure 8 displays the best parameters and the CV performance. We found that the best single-scale exponential model is $\text{ecifGGL}_{17.5,1.5}^{\text{E}}$ with median $R_p=0.739$ (Figure 8a) and the best single-scale Lorentz kernel model is $\text{ecifGGL}_{15.5,1.5}^{\text{L}}$ with median $R_p=0.738$ (Figure 8b). The best two-scale exponential kernel model is found to be $\text{ecifGGL}_{17.5,1.5;16.5,8.5}^{\text{E,E}}$ with median $R_p=0.741$ (Figure 8c). Finally, (Figure 8d), shows that the best two-scale Lorentz kernel model is $\text{ecifGGL}_{15.5,1.5;15.0,7.5}^{\text{L,L}}$ with median $R_p=0.742$.

Having optimized the models’ hyperparameters, we now predict the binding affinity of the 195 complexes in the CASF-2007 test set. Just like in the previous two benchmarks, we first train each model using the smaller training set S_R and produce a prediction for the test set from the average of 50 runs. Secondly, we use the bigger training set S_G of this benchmark, which is the PDBbind v2007 general set excluding the CASF-2007 core set, to train the model and use the trained model to predict the binding affinity of the test set.

The performance of all our selected models for this benchmark is reported in Table 4. We observe that all of these models perform significantly better when trained with the bigger training set S_G . Following a similar trend as in the previous two benchmarks, the SYBYL atom-type models of this benchmark consistently perform better than their ECIF atom-type counterparts. Also, the two-scale kernel model improves the performance compared to their single-scale versions. The best-performing model for this benchmark is the two-scale Lorentz kernel SYBYL atom-type model $\text{sybylGGL}_{13.5,0.5;13.0,9.5}^{\text{L,L}}$ with Pearson’s correlation coefficient $R_p=0.834$. Moreover, Figure 9a reveals the scoring power of our model in this benchmark. Our proposed GGL model stands at the top with reported $R_p=0.834$ while AGL-Score is the runner-up with $R_p=0.830$.

Table 4: Performance of various GGL models on CASF-2007 test set.

Pearson’s R_p of single-scale Model			Pearson’s R_p of two-scale Model	
Model	Trained with S_R	Trained with S_G	Model	Trained with S_G
$\text{sybylGGL}_{2.5,0.5}^{\text{E}}$	0.803	0.824	$\text{sybylGGL}_{2.5,0.5;19.0,9.0}^{\text{E,E}}$	0.833
$\text{sybylGGL}_{13.5,0.5}^{\text{L}}$	0.807	0.827	$\text{sybylGGL}_{13.5,0.5;13.0,9.5}^{\text{L,L}}$	0.834
$\text{ecifGGL}_{17.5,1.5}^{\text{E}}$	0.794	0.807	$\text{ecifGGL}_{17.5,1.5;16.5,8.5}^{\text{E,E}}$	0.811
$\text{ecifGGL}_{15.5,1.5}^{\text{L}}$	0.792	0.805	$\text{ecifGGL}_{15.5,1.5;15.0,7.5}^{\text{L,L}}$	0.809

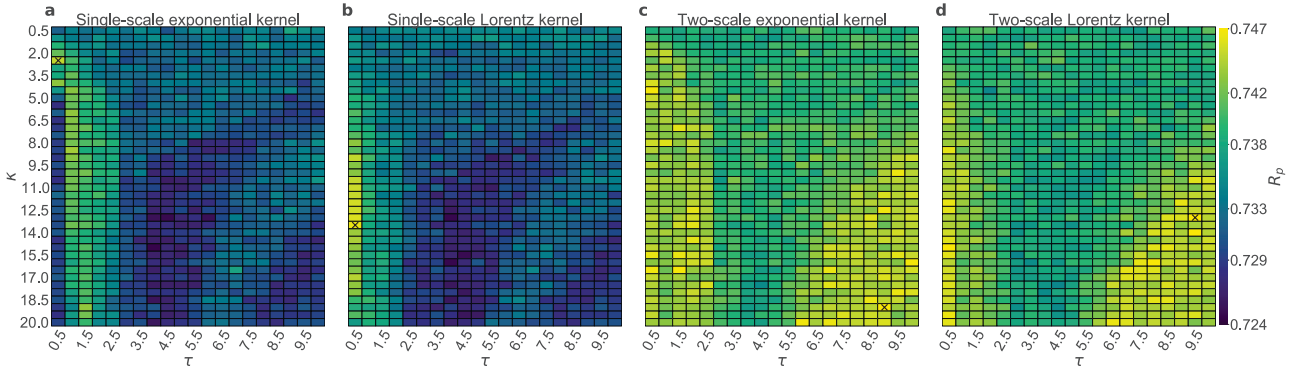


Figure 7: Optimized parameters for sybylGGL model for CASF-2007 benchmark. The best parameters locations are marked by “x”. The optimal parameters for (a) single-scale exponential kernel model are $(\kappa, \tau) = (2.5, 0.5)$ with the corresponding median $R_p = 0.745$ and (b) single-scale Lorentz kernel model are $(\kappa, \tau) = (13.5, 0.5)$ with corresponding median $R_p = 0.746$. The optimal second kernel parameters for (c) two-scale exponential kernel model are $(\kappa, \tau) = (19.0, 9.0)$ with the corresponding median $R_p = 0.747$ and (d) two-scale Lorentz kernel model are $(\kappa, \tau) = (13.0, 9.5)$ with the corresponding median $R_p = 0.747$.

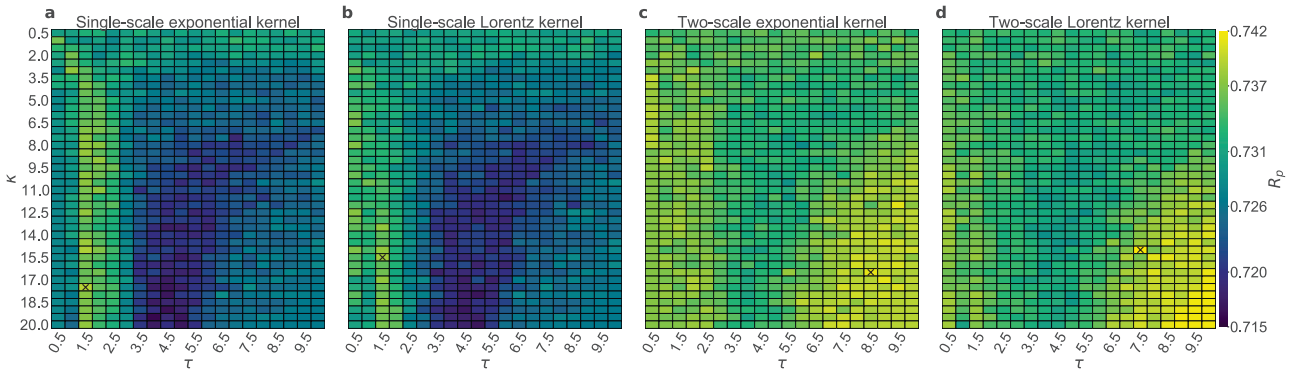


Figure 8: Optimized parameters for ecifGGL model for CASF-2007 benchmark. The best parameters locations are marked by “x”. The optimal parameters for (a) single-scale exponential kernel model are $(\kappa, \tau) = (17.5, 1.5)$ with the corresponding median $R_p = 0.739$ and (b) single-scale Lorentz kernel model are $(\kappa, \tau) = (15.5, 1.5)$ with corresponding median $R_p = 0.738$. The optimal second kernel parameters for (c) two-scale exponential kernel model are $(\kappa, \tau) = (16.5, 8.5)$ with the corresponding median $R_p = 0.741$ and (d) two-scale Lorentz kernel model are $(\kappa, \tau) = (15.0, 7.5)$ with the corresponding median $R_p = 0.742$.

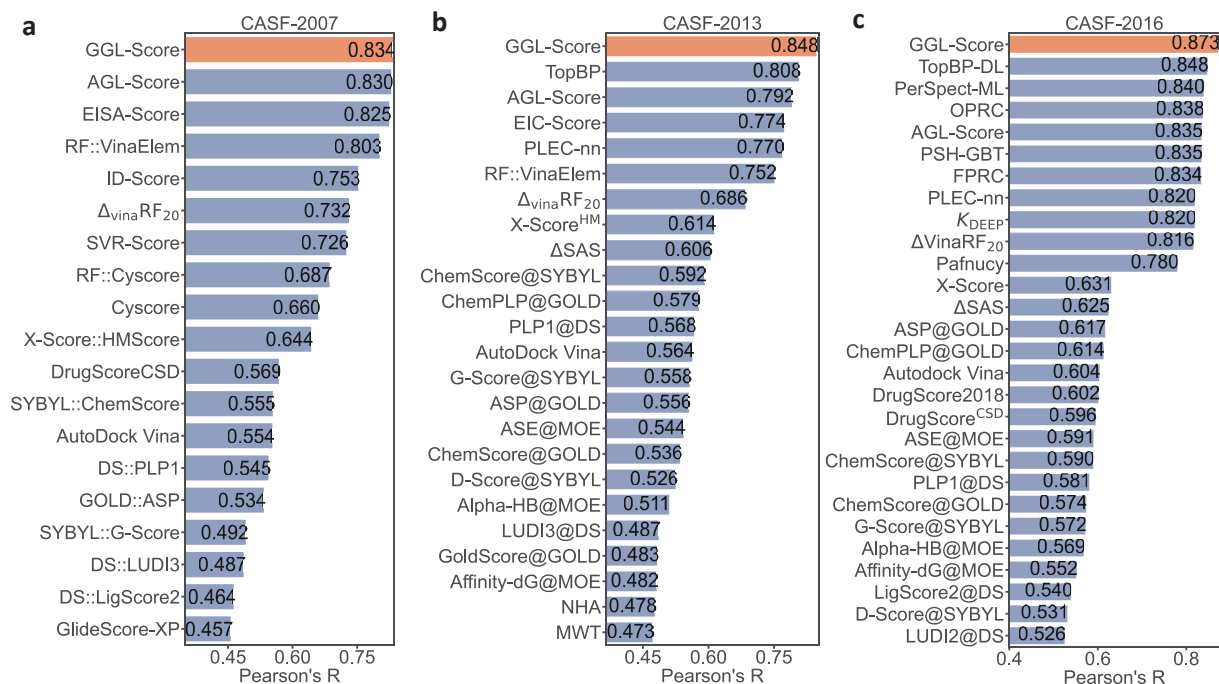


Figure 9: Performance comparison of different scoring functions on CASF benchmarks. Our proposed model in this work, GGL-Score, is highlighted in red, and the rest is in purple. a) CASF-2007: the performances of other methods taken from previous studies [33, 31, 44, 45, 46, 47, 48]. Our ^{sybyl}GGL-Score achieves $R_p=0.834$ b) CASF-2013: the other results are extracted from [48, 40, 45]. Our ^{sybyl}GGL-Score achieves $R_p=0.848$. c) CASF-2016: our ^{sybyl}GGL-Score achieves $R_p=0.873$, other scoring functions are discussed in [41, 49, 48].

4 Conclusion

The binding affinity between a ligand and its receptor protein is a key component in structure-based drug design. Although significant progress has been made over the past decades, an accurate prediction of protein-ligand binding affinity remains a challenging task. Geometric graph theories are widely used in the study of molecular and biomolecular systems. Furthermore, the element-type graph coloring-based multiscale weighted colored graph (MWCG) approaches have particularly shown success in the task of binding affinity prediction [1, 2]. On the other hand, SYBYL atom-type interaction and extended connectivity interactive features (ECIF) have enjoyed their success in molecular property prediction [32, 35]. Therefore, with an aim to develop robust and reliable scoring functions for large and diverse protein-ligand datasets, the present work combines the graph learning model and extended atom types to give rise to novel geometric graph theory-based multiscale weighted colored graph (MWCG) descriptors for the protein-ligand complex where the graph coloring is based on SYBYL atom-type and ECIF atom-type interactions. By pairing with the gradient boosting decision tree (GBDT) machine learning algorithm, our approach results in two different methods, namely ^{sybyl}GGL-Score and ^{ecif}GGL-Score. We explore the optimal hyperparameters of our models using a five-fold cross-validation on the training set of three commonly used benchmarks in drug design area, namely CASF-2007 [33], CASF-2013 [40], and CASF-2016 [41]. For the binding affinity prediction task of each benchmark’s test set complexes, we consider two training sets– the refined set excluding the core set and the general set excluding the core set. Our model performs significantly better in each benchmark when trained with the larger training set. It is also found that the SYBYL atom-type models ^{sybyl}GGL-Score outperform the ECIF atom-type models ^{ecif}GGL-Score in most cases.

To demonstrate the scoring power of the proposed models, many state-of-the-art scoring functions are considered in each benchmark. Impressively, our ^{sybyl}GGL-Score outperforms other models by a wide margin in all three PDBbind benchmarks. In addition to the accuracy and robustness, our model is computationally inexpensive– the only required structural input is the atom types and coordinates. Moreover, our model can be applied in a vast majority of molecular property predictions such as toxicity, solubility, protein mutation, protein folding, and protein-nucleic acid interactions.

5 Appendix A

In this section, we explore the performance of the basic geometric graph approach model that considers element-type interactions presented in [1] using the bigger training set S_G , i.e. the general set excluding the core set of each benchmark. We carry out a similar experiment as we did for our present model. For simplicity, we use the notation $\text{GGL}_{\kappa,\tau}^\alpha$ for a single-scale kernel and $\text{GGL}_{\kappa_1,\tau_1;\kappa_2,\tau_2}^{\alpha_1,\alpha_2}$ for a two-scale kernel basic element-type geometric graph learning model. To find the optimized parameters for each benchmark, we carry out a five-fold CV on the training set S_R i.e. the refined set excluding the core set of the corresponding benchmark. For CASF-2016 benchmark, the best single kernel models are

found to be $\text{GGL}_{3.5,2.0}^E$ (Figure A1a) and $\text{GGL}_{16.0,2.0}^L$ (Figure A1b) with median Pearson correlation $R_p=0.769$ for both models. The best two kernel models for CASF–2016 are $\text{GGL}_{3.5,2.0;16.0,3.0}^{E,E}$ (Figure A1c) and $\text{GGL}_{16.0,2.0;12.0,1.5}^{L,L}$ (Figure A1d) with median $R_p=0.773$ for both models. The performance of all models on the test set of CASF–2016 benchmark are reported in Table A1. It is interesting to find that the performance of each model improved significantly when trained with the bigger training data S_G i.e. PDBbind v2016 general set excluding the core set. The best performing model for this benchmark is the two-scale exponential kernel model $\text{GGL}_{3.5,2.0;16.0,3.0}^{E,E}$ with $R_p=0.859$. We note that both of our proposed GGL models, SYBYL atom-type and ECIF atom-type model, perform promisingly better (with reported $R_p=0.873$ and 0.868 respectively) than the basic element-type model.

The CV performance of CASF–2013 benchmark (Figure A2), reveals that the best models for this benchmark are $\text{GGL}_{5.0,2.0}^E$ and $\text{GGL}_{16.0,2.0}^L$ for the single kernel, and $\text{GGL}_{5.0,2.0;15.0,3.0}^{E,E}$ and $\text{GGL}_{16.0,2.0;11.5,1.5}^{L,L}$ for two kernels, with median $R_p=0.774, 0.773, 0.778,$ and 0.776 , respectively. Table A1 indicates that the use of the bigger training set S_G improved the performance of these models. The best performing model for this benchmark is the single-scale exponential model $\text{GGL}_{5.0,2.0}^E$ with reported $R_p=0.821$. However, our proposed SYBYL atom-type GGL model outperforms the basic GGL model by a huge margin with reported $R_p=0.848$ for this benchmark.

Figure A3 plots the CV performance for CASF–2007 benchmark. The best models for this benchmark are $\text{GGL}_{17.0,1.5}^E$ and $\text{GGL}_{17.0,1.5}^L$ for the single kernel, and $\text{GGL}_{17.0,1.5;16.5,3.0}^{E,E}$ and $\text{GGL}_{17.0,1.5;6.5,10.0}^{L,L}$ for two kernels, with median $R_p=0.724, 0.724, 0.733,$ and 0.730 , respectively. The performance of these models is presented in Table A1. We observe that the use of the bigger training data significantly improves the performance of each model for this benchmark as well. While the best performing basic GGL model for this benchmark is the two-scale exponential kernel model $\text{GGL}_{17.0,1.5;16.5,3.0}^{E,E}$ with Pearson’s $R_p=0.833$, our proposed SYBYL atom-type GGL model for this benchmark perform slightly better with $R_p=0.834$.

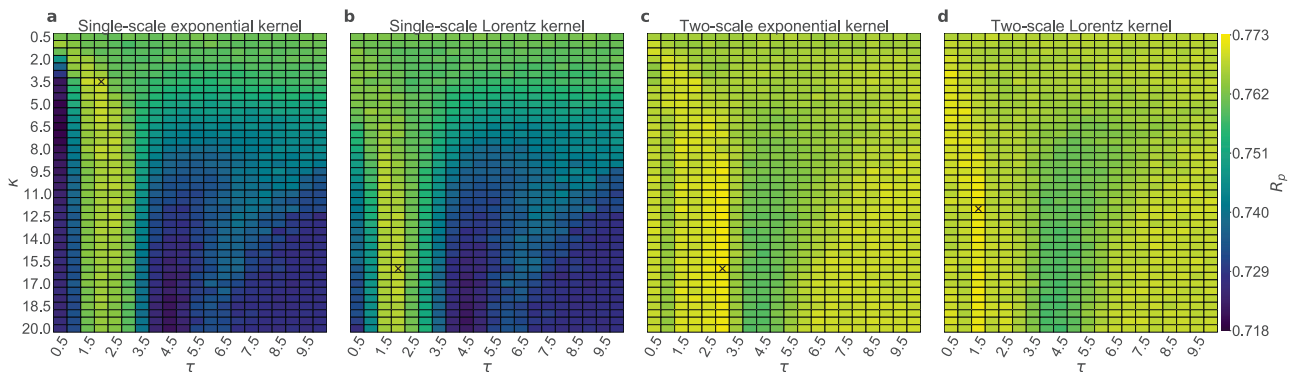


Figure A1: Optimized parameters for basic GGL model for CASF–2016 benchmark. The best parameters locations are marked by “x”. The optimal parameters for (a) single-scale exponential kernel model are $(\kappa, \tau) = (3.5, 2.0)$ with the corresponding median $R_p = 0.769$ and (b) single-scale Lorentz kernel model are $(\kappa, \tau) = (16.0, 2.0)$ with corresponding median $R_p = 0.769$. The optimal second kernel parameters for (c) two-scale exponential kernel model are $(\kappa, \tau) = (16.0, 3.0)$ with the corresponding median $R_p = 0.773$ and (d) two-scale Lorentz kernel model are $(\kappa, \tau) = (12.0, 1.5)$ with the corresponding median $R_p = 0.773$.

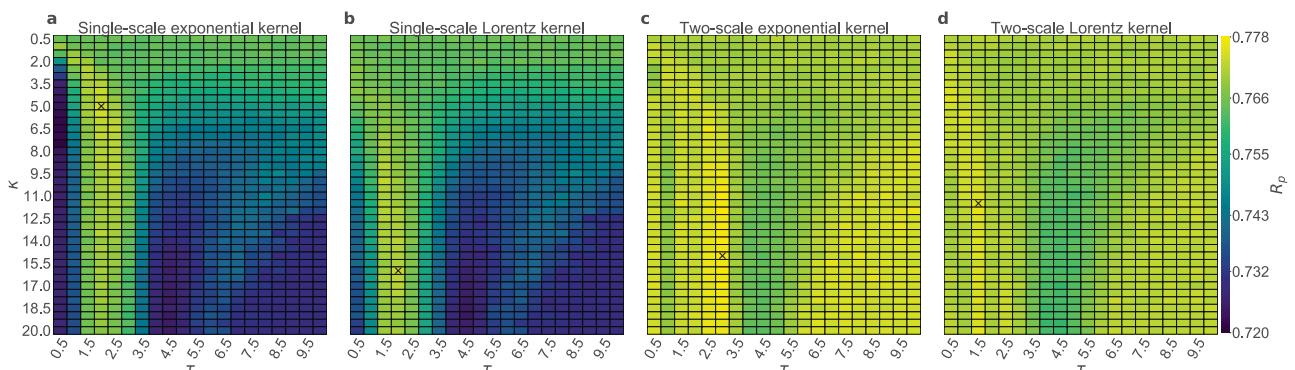


Figure A2: Optimized parameters for basic GGL model for CASF–2013 benchmark. The best parameters locations are marked by “x”. The optimal parameters for (a) single-scale exponential kernel model are $(\kappa, \tau) = (5.0, 2.0)$ with the corresponding median $R_p = 0.774$ and (b) single-scale Lorentz kernel model are $(\kappa, \tau) = (16.0, 2.0)$ with corresponding median $R_p = 0.773$. The optimal second kernel parameters for (c) two-scale exponential kernel model are $(\kappa, \tau) = (15.0, 3.0)$ with the corresponding median $R_p = 0.778$ and (d) two-scale Lorentz kernel model are $(\kappa, \tau) = (11.5, 1.5)$ with the corresponding median $R_p = 0.776$.

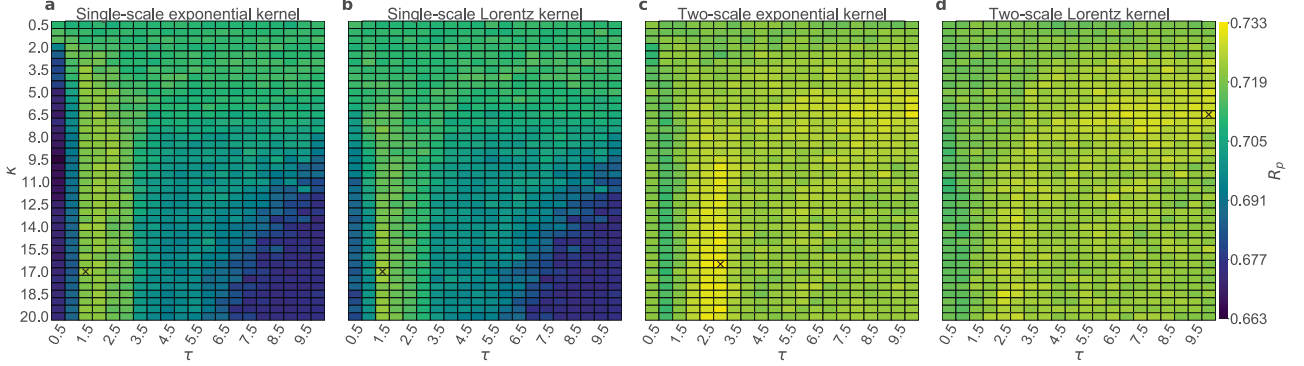


Figure A3: Optimized parameters for basic GGL model for CASF-2007 benchmark. The best parameters locations are marked by “x”. The optimal parameters for (a) single-scale exponential kernel model are $(\kappa, \tau) = (17.0, 1.5)$ with the corresponding median $R_p = 0.724$ and (b) single-scale Lorentz kernel model are $(\kappa, \tau) = (17.0, 1.5)$ with corresponding median $R_p = 0.724$. The optimal second kernel parameters for (c) two-scale exponential kernel model are $(\kappa, \tau) = (16.5, 3.0)$ with the corresponding median $R_p = 0.733$ and (d) two-scale Lorentz kernel model are $(\kappa, \tau) = (6.5, 10.0)$ with the corresponding median $R_p = 0.730$.

Table A1: Performance of various basic GGL models on all benchmark test sets.

	Pearson's R_p of single-scale Model			Pearson's R_p of two-scale Model	
	Model	Trained with S_R	Trained with S_G	Model	Trained with S_G
CASF-2016	$\text{GGL}_{3.5,2.0}^E$	0.843	0.856	$\text{GGL}_{3.5,2.0;16.0,3.0}^{E,E}$	0.859
	$\text{GGL}_{16.0,2.0}^L$	0.839	0.848	$\text{GGL}_{16.0,2.0;12.0,1.5}^{L,L}$	0.856
CASF-2013	$\text{GGL}_{5.0,2.0}^E$	0.794	0.821	$\text{GGL}_{5.0,2.0;15.0,3.0}^{E,E}$	0.818
	$\text{GGL}_{16.0,2.0}^L$	0.793	0.809	$\text{GGL}_{16.0,2.0;11.5,1.5}^{L,L}$	0.818
CASF-2007	$\text{GGL}_{17.0,1.5}^E$	0.809	0.828	$\text{GGL}_{17.0,1.5;16.5,3.0}^{E,E}$	0.833
	$\text{GGL}_{17.0,1.5}^L$	0.815	0.830	$\text{GGL}_{17.0,1.5;6.5,10.0}^{L,L}$	0.830

6 Data and Software Availability

The source code is available at Github: <https://github.com/NguyenLabUKY/GGL-ETA-Score>.

7 Competing interests

No competing interest is declared.

8 Acknowledgments

This work is supported in part by funds from the National Science Foundation (NSF: # 2053284 and # 2151802), and University of Kentucky Startup Fund.

References

- [1] Duc D Nguyen, Tian Xiao, Menglun Wang, and Guo-Wei Wei. Rigidity strengthening: A mechanism for protein–ligand binding. *Journal of chemical information and modeling*, 57(7):1715–1721, 2017.
- [2] Duc Duy Nguyen and Guo-Wei Wei. Agl-score: algebraic graph learning score for protein–ligand binding scoring, ranking, docking, and screening. *Journal of chemical information and modeling*, 59(7):3291–3304, 2019.
- [3] Dong Chen, Kaifu Gao, Duc Duy Nguyen, Xin Chen, Yi Jiang, Guo-Wei Wei, and Feng Pan. Algebraic graph-assisted bidirectional transformers for molecular property prediction. *Nature Communications*, 12(1):1–9, 2021.
- [4] Rui Wang, Duc Duy Nguyen, and Guo-Wei Wei. Persistent spectral graph. *International journal for numerical methods in biomedical engineering*, 36(9):e3376, 2020.
- [5] Zhenyu Meng and Kelin Xia. Persistent spectral–based machine learning (perspect ml) for protein–ligand binding affinity prediction. *Science Advances*, 7(19):eabc5329, 2021.
- [6] Nenad Trinajstić. *Chemical graph theory*. CRC press, 2018.
- [7] Harry P Schultz. Topological organic chemistry. 1. graph theory and topological indices of alkanes. *Journal of Chemical Information and Computer Sciences*, 29(3):227–228, 1989.
- [8] Dusanka Janežić, Ante Milicević, Sonja Nikolić, and Nenad Trinajstić. *Graph-theoretical matrices in chemistry*. CRC Press, 2015.
- [9] A Angeleska, N Jonoska, and M Saito. Dna rearrangement through assembly graphs. *Discrete. Appl. Math.*, 157:3020–3037, 2009.
- [10] N. Go, T. Noguti, and T. Nishikawa. Dynamics of a small globular protein in terms of low-frequency vibrational modes. *Proc. Natl. Acad. Sci.*, 80:3696 – 3700, 1983.
- [11] M. Tasumi, H. Takenchi, S. Ataka, A. M. Dwidedi, and S. Krimm. Normal vibrations of proteins: Glucagon. *Biopolymers*, 21:711 – 714, 1982.
- [12] Bernard R Brooks, Robert E Bruccoleri, Barry D Olafson, David J States, S a Swaminathan, and Martin Karplus. Charmm: a program for macromolecular energy, minimization, and dynamics calculations. *Journal of computational chemistry*, 4(2):187–217, 1983.
- [13] Michael Levitt, Christian Sander, and Peter S Stern. Protein normal-mode dynamics: trypsin inhibitor, crambin, ribonuclease and lysozyme. *Journal of molecular biology*, 181(3):423–447, 1985.
- [14] Ivet Bahar, Ali Rana Atilgan, and Burak Erman. Direct evaluation of thermal fluctuations in proteins using a single-parameter harmonic potential. *Folding and Design*, 2(3):173–181, 1997.
- [15] Paul J Flory. Statistical thermodynamics of random networks. *Proceedings of the Royal Society of London. A. Mathematical and Physical Sciences*, 351(1666):351–380, 1976.
- [16] Ivet Bahar, Ali Rana Atilgan, Melik C Demirel, and Burak Erman. Vibrational dynamics of folded proteins: significance of slow and fast motions in relation to function and stability. *Physical Review Letters*, 80(12):2733, 1998.
- [17] Ali Rana Atilgan, SR Durell, Robert L Jernigan, Melik C Demirel, O Keskin, and Ivet Bahar. Anisotropy of fluctuation dynamics of proteins with an elastic network model. *Biophysical journal*, 80(1):505–515, 2001.
- [18] Konrad Hinsén. Analysis of domain motions by approximate normal mode calculations. *Proteins: Structure, Function, and Bioinformatics*, 33(3):417–429, 1998.
- [19] Florence Tama and Y-H Sanejouand. Conformational change of proteins arising from normal mode calculations. *Protein engineering*, 14(1):1–6, 2001.
- [20] Kelin Xia, Kristopher Opron, and Guo-Wei Wei. Multiscale multiphysics and multidomain models—flexibility and rigidity. *The Journal of chemical physics*, 139(19):11B614_1, 2013.
- [21] Kristopher Opron, Kelin Xia, and Guo-Wei Wei. Fast and anisotropic flexibility–rigidity index for protein flexibility and fluctuation analysis. *The Journal of chemical physics*, 140(23):06B617_1, 2014.

- [22] Kristopher Opron, Kelin Xia, Zach Burton, and Guo-Wei Wei. Flexibility–rigidity index for protein–nucleic acid flexibility and fluctuation analysis. *Journal of computational chemistry*, 37(14):1283–1295, 2016.
- [23] Duc Duy Nguyen, Kelin Xia, and Guo-Wei Wei. Generalized flexibility-rigidity index. *The Journal of chemical physics*, 144(23):234106, 2016.
- [24] Kristopher Opron, Kelin Xia, and Guo-Wei Wei. Communication: Capturing protein multiscale thermal fluctuations. *The Journal of chemical physics*, 142(21):06B401_1, 2015.
- [25] David Bramer and Guo-Wei Wei. Multiscale weighted colored graphs for protein flexibility and rigidity analysis. *The Journal of chemical physics*, 148(5):054103, 2018.
- [26] Duc Duy Nguyen, Zixuan Cang, Kedi Wu, Menglun Wang, Yin Cao, and Guo-Wei Wei. Mathematical deep learning for pose and binding affinity prediction and ranking in d3r grand challenges. *Journal of computer-aided molecular design*, 33(1):71–82, 2019.
- [27] Duc Duy Nguyen, Kaifu Gao, Menglun Wang, and Guo-Wei Wei. Mathdl: mathematical deep learning for d3r grand challenge 4. *Journal of computer-aided molecular design*, 34(2):131–147, 2020.
- [28] Zied Gaieb, Shuai Liu, Symon Gathiaka, Michael Chiu, Huanwang Yang, Chenghua Shao, Victoria A Feher, W Patrick Walters, Bernd Kuhn, and Markus G Rudolph. D3r grand challenge 2: blind prediction of protein–ligand poses, affinity rankings, and relative binding free energies. *Journal of computer-aided molecular design*, 32(1):1–20, 2018.
- [29] Zied Gaieb, Conor Parks, Michael Chiu, Huanwang Yang, Chenghua Shao, Patrick Walters, Millard Lambert, Neysa Nevins, Scott D Bembenek, and Stephen K Burley. D3r grand challenge 3: Blind prediction of protein-ligand poses and affinity rankings. *Journal of computer-aided molecular design*, 33(1):1–18, 2018.
- [30] Conor D Parks, Zied Gaieb, Michael Chiu, Huanwang Yang, Chenghua Shao, W Patrick Walters, Johanna M Jansen, Georgia McGaughey, Richard A Lewis, and Scott D Bembenek. D3r grand challenge 4: blind prediction of protein–ligand poses, affinity rankings, and relative binding free energies. *Journal of computer-aided molecular design*, 34(2):99–119, 2020.
- [31] Pedro J Ballester and John BO Mitchell. A machine learning approach to predicting protein–ligand binding affinity with applications to molecular docking. *Bioinformatics*, 26(9):1169–1175, 2010.
- [32] Pedro J Ballester, Adrian Schreyer, and Tom L Blundell. Does a more precise chemical description of protein–ligand complexes lead to more accurate prediction of binding affinity? *Journal of chemical information and modeling*, 54(3):944–955, 2014.
- [33] Tiejun Cheng, Xun Li, Yan Li, Zhihai Liu, and Renxiao Wang. Comparative assessment of scoring functions on a diverse test set. *Journal of chemical information and modeling*, 49(4):1079–1093, 2009.
- [34] Maciej Wójcikowski, Michał Kukielka, Marta M Stepniewska-Dziubinska, and Paweł Siedlecki. Development of a protein–ligand extended connectivity (plec) fingerprint and its application for binding affinity predictions. *Bioinformatics*, 35(8):1334–1341, 2019.
- [35] Norberto Sánchez-Cruz, José L Medina-Franco, Jordi Mestres, and Xavier Barril. Extended connectivity interaction features: improving binding affinity prediction through chemical description. *Bioinformatics*, 37(10):1376–1382, 2021.
- [36] David Rogers and Mathew Hahn. Extended-connectivity fingerprints. *Journal of chemical information and modeling*, 50(5):742–754, 2010.
- [37] Duc Duy Nguyen and Guo-Wei Wei. DG-GL: differential geometry-based geometric learning of molecular datasets. *International journal for numerical methods in biomedical engineering*, 35(3):e3179, 2019.
- [38] Md Masud Rana and Duc Duy Nguyen. Eisa-score: Element interactive surface area score for protein-ligand binding affinity prediction. *arXiv preprint arXiv:2206.00611*, 2022.
- [39] Zixuan Cang and Guo-Wei Wei. Integration of element specific persistent homology and machine learning for protein-ligand binding affinity prediction. *International journal for numerical methods in biomedical engineering*, 34(2):e2914, 2018.
- [40] Yan Li, Li Han, Zhihai Liu, and Renxiao Wang. Comparative assessment of scoring functions on an updated benchmark: 2. evaluation methods and general results. *Journal of chemical information and modeling*, 54(6):1717–1736, 2014.
- [41] Minyi Su, Qifan Yang, Yu Du, Guoqin Feng, Zhihai Liu, Yan Li, and Renxiao Wang. Comparative assessment of scoring functions: the casf-2016 update. *Journal of chemical information and modeling*, 59(2):895–913, 2018.
- [42] Jian Jiang, Rui Wang, and Guo-Wei Wei. Ggl-tox: geometric graph learning for toxicity prediction. *Journal of chemical information and modeling*, 61(4):1691–1700, 2021.
- [43] Kelin Xia, Kristopher Opron, and Guo-Wei Wei. Multiscale gaussian network model (mgnm) and multiscale anisotropic network model (manm). *The Journal of chemical physics*, 143(20):11B616_1, 2015.
- [44] Guo-Bo Li, Ling-Ling Yang, Wen-Jing Wang, Lin-Li Li, and Sheng-Yong Yang. Id-score: a new empirical scoring function based on a comprehensive set of descriptors related to protein–ligand interactions. *Journal of chemical information and modeling*, 53(3):592–600, 2013.

- [45] Hongjian Li, Kwong-Sak Leung, Man-Hon Wong, and Pedro J Ballester. Improving autodock vina using random forest: the growing accuracy of binding affinity prediction by the effective exploitation of larger data sets. *Molecular informatics*, 34(2-3):115–126, 2015.
- [46] Hongjian Li, Kwong-Sak Leung, Man-Hon Wong, and Pedro J Ballester. Substituting random forest for multiple linear regression improves binding affinity prediction of scoring functions: Cyscore as a case study. *BMC bioinformatics*, 15(1):1–12, 2014.
- [47] Yang Cao and Lei Li. Improved protein–ligand binding affinity prediction by using a curvature-dependent surface-area model. *Bioinformatics*, 30(12):1674–1680, 2014.
- [48] Cheng Wang and Yingkai Zhang. Improving scoring-docking-screening powers of protein–ligand scoring functions using random forest. *Journal of computational chemistry*, 38(3):169–177, 2017.
- [49] Marta M Stepniewska-Dziubinska, Piotr Zielenkiewicz, and Pawel Siedlecki. Development and evaluation of a deep learning model for protein-ligand binding affinity prediction. *Bioinformatics*, 1:9, 2018.